Table 1 Comparison of guidance laws

Time, sec	Acceleration command, fps		Time-to-go, sec		Number of iterations
	WEBON	PPN	WEBON	PPN	
0.1	−934	−873	0.9530	0.9574	4
0.2	−1,030	−961	0.8539	0.8576	4
0.3	−983	−933	0.7547	0.7572	4
0.4	−882	−864	0.6554	0.6568	4
0.5	−757	−774	0.5559	0.5565	4
0.6	−599	−670	0.4562	0.4563	3
0.7	−404	−552	0.3564	0.3563	3
0.8	−164	−419	0.2565	0.2564	3
0.9	163	−257	0.1566	0.1565	3
1.0	633	58	0.0566	0.0565	2

At intercept: Guidance scheme	Time, sec	g-s	Miss, ft
WEBON	1.057	18.5	1.5
PPN	1.057	19.4	1.7

less stringent conditions. Thus, engagements between a very fast interceptor (~ 10 kfps) and a target with velocity superiority of up to 2:1 were simulated. The geometry of an actual engagement simulated is depicted in Figure 2. The origin of the coordinate frame is at an altitude of approximately 25 kft and the total duration of the engagement is just over one second. Thus WEBON was tested here in the role of homing guidance. For economical reasons, only deterministic cases were considered here.

Results

Trajectories for a simulated engagement are shown in Fig. 2. The corresponding interceptor acceleration command histories obtained with PPN as well as WEBON guidance are shown in Fig. 3. Table 1 presents a numerical comparison of these guidance commands showing, in addition, a comparison of the time-to-go estimates as a function of engagement time, and the number of iterations required for convergence by the presented guidance scheme.

In spite of the comparison against a very sophisticated guidance scheme, the results obtained were encouraging. The energy loss due to drag was, as in the case shown in Table 1, reduced in all cases considered. This reduction would be more pronounced against simpler guidance schemes, such as proportional navigation. The fact that atmospheric density had to be assumed constant to obtain the closed form solution presented may account for part of the difference shown in the initial estimates of $\hat{t}_f$, but this did not prove detrimental.

Mechanical Behavior of Fiber Reinforced Cylindrical Shells

J. PADOVAN* AND J. LESTINGI†
University of Akron, Akron, Ohio

To date, the effects of material anisotropy on the static behavior of cylindrical shells has been studied by several investigators.[1–4] In all of these analyses though, no numerical results are available for the case of nonsymmetric loading of such shells. The present Note studies the mechanical response of a statically loaded, fiber-reinforced cylindrical shell with arbitrary boundary conditions. Specifically, the effects of fiber orientation on the shell stress, strain and displacement fields of the cylinder are discussed in detail. Since the cylinder is fiber-reinforced, the material properties are characterized as a generalized Hookean material characteristic of anisotropic shell theory.

The position of a point of a cylindrical shell is given by β the circumferential variable, x the axial distance, and z the coordinate normal to the middle surface. Furthermore, R is the radius of the cylinder, H the thickness, and L the length. Since the cylinder coordinates (x, β) generally do not line up with the fiber directions, the 3-D constitutive equations will have certain anisotropic compliances included. As shear deformation is admitted in the present analysis, the constitutive equations appropriate to the cylindrical shell have the form

$$\begin{bmatrix}\sigma_{xx}\\ \sigma_{\beta\beta}\\ \sigma_{x\beta}\\ \sigma_{\beta z}\\ \sigma_{zx}\end{bmatrix} = \begin{bmatrix} E_{11} & E_{12} & E_{13} & 0 & 0\\ & E_{22} & E_{24} & 0 & 0\\ & & E_{44} & 0 & 0\\ & & & E_{55} & E_{56}\\ & & & & E_{66}\end{bmatrix}\begin{bmatrix}\varepsilon_{xx}\\ \varepsilon_{\beta\beta}\\ \varepsilon_{x\beta}\\ \varepsilon_{\beta z}\\ \varepsilon_{zx}\end{bmatrix} \tag{1}$$

where $\sigma_{xx},\ldots$ and $\varepsilon_{xx},\ldots$ are 3-D stresses and strains.

Since shear deformation is admitted, the shell strains and stresses are given by

$$\varepsilon_{xx} = u,_x^{(0)} + zu,_x^{(1)} \tag{2a}$$

$$\varepsilon_{\beta\beta} = [1/(R+z)]v,_\beta^{(0)} + [z/(R+z)]v,_\beta^{(1)} + [1/(R+z)]w^{(0)} \tag{2b}$$

$$\varepsilon_{x\beta} = [1(R+z)]u,_\beta^{(0)} + [z/(R+z)]u,_\beta^{(1)} + v,_x^{(0)} + zv,_x^{(1)} \tag{2c}$$

$$\varepsilon_{\beta z} = [1/(R+z)]w,_\beta^{(0)} - [1/(R+z)]v^{(0)} - [z/(R-z)]v^{(1)} + v^{(1)} \tag{2d}$$

$$\varepsilon_{zx} = u^{(1)} + w,_x^{(0)} \tag{2e}$$

$$\{\sigma_{xx}^{(0)}, \sigma_{x\beta}^{(0)}, \sigma_{zx}^{(0)}; \sigma_{xx}^{(0)}, \sigma_{x\beta}^{(1)}\} = <(\sigma_{xx}, \sigma_{x\beta}, \sigma_{zx})(R+z)(1;z)> \tag{3a}$$

$$\{\sigma_{\beta x}^{(0)}\ \sigma_{\beta\beta}^{(0)}, \sigma_{\beta z}^{(0)}; \sigma_{\beta x}^{(1)}, \sigma_{\beta\beta}^{(1)}\} = <(\sigma_{\beta x}, \sigma_{\beta\beta}, \sigma_{\beta x})(1;z)> \tag{3b}$$

For notational convenience ( ), x and ( ), β denote partial differentiation with respect to x and β and $< >$ is defined by‡

$$\langle\ \rangle = \int_{-H/2}^{+H/2} (\ )\,dz \tag{4}$$

Furthermore, $u^{(0)}$, $v^{(0)}$, and $w^{(0)}$ are the shell displacements of the middle surface in the x, β and z directions and $u^{(1)}$, $v^{(1)}$ are the rotations of the normal to the middle surface in the x and β directions. For the material properties characterized by Eq. (1), the displacement equilibrium equations can be written as[6]

$$B_1\boldsymbol{\zeta},_{xx} + B_2\boldsymbol{\zeta},_{\beta\beta} + B_3\boldsymbol{\zeta},_{x\beta} + B_4\boldsymbol{\zeta},_x + B_5\boldsymbol{\zeta},_\beta + B_6\boldsymbol{\zeta} + \mathbf{F} = \mathbf{0} \tag{5}$$

where the coefficients B_l, $l = 1, 2, \ldots, 6$ are five by five matrices such that B_1, B_2, B_3 and B_6 are Hermitian while B_4 and B_5 are

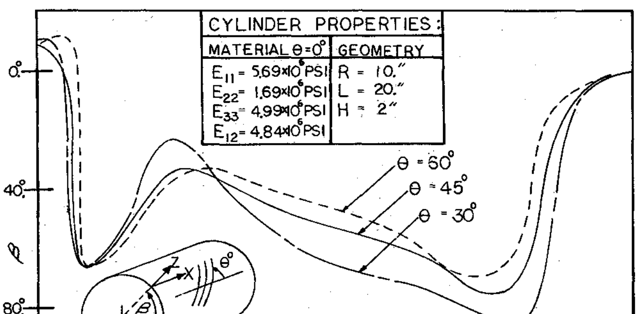

Fig. 1 Loci of the maximum value of $\sigma_{xz}^{(1)}$ for several values of θ.

‡ The integration defined by Eq. (4) is performed in the manner of Flügge second order theory.[5]

Received December 1, 1971; revision received April 19, 1972.
Index categories: Structural Composite Materials (Including Coatings); Structural Static Analysis.

* Assistant Professor of Mechanical Engineering.
† Associate Professor of Civil Engineering.

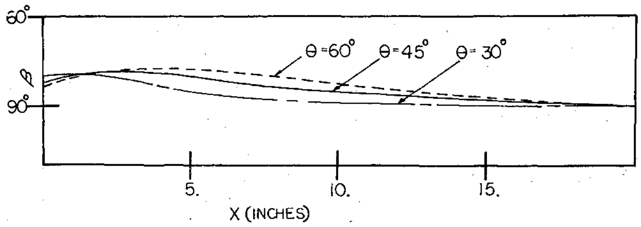

Fig. 2 Loci of the maximum value of $w^{(0)}$ for several values of θ.

negative symmetric. Furthermore, the transpose of $\boldsymbol{\zeta}$ and the column vector $\mathbf{F}$ are given by

$$\zeta^T = \{u^{(0)}, u^{(1)}, v^{(0)}, v^{(1)}, w^{(0)}\} \tag{6}$$

$$\mathbf{F} = \begin{bmatrix} (R+H)\sigma_{zx}|_{z=H/2} & -\,(R-H)\sigma_{zx}|_{z=-H/2} \\ (R+H)H\sigma_{zx}|_{z=H/2} & +\,(R-H)H\sigma_{zx}|_{z=-H/2} \\ (R+H)\sigma_{z\beta}|_{z=H/2} & -\,(R-H)\sigma_{z\beta}|_{z=-H/2} \\ (R+H)H\sigma_{z\beta}|_{z=H/2} & +\,(R-H)H\sigma_{z\beta}|_{z=-H/2} \\ (R+H)\sigma_{zz}|_{z=H/2} & -\,(R-H)\sigma_{zz}|_{z=-H/2} \end{bmatrix} \tag{7}$$

The boundary conditions associated with Eqs. (5) for the $x = 0$ and L faces are given by

$$\sigma_{xx}^{(i)}|_{x=0,L} = \tilde{\sigma}_{xx}^{(i)} \text{ or } u^{(i)} \text{ are prescribed} \tag{8a}$$

$$\sigma_{x\beta}^{(i)}|_{x=0,L} = \tilde{\sigma}_{x\beta}^{(i)} \text{ or } v^{(i)} \text{ are prescribed} \tag{8b}$$

$$\sigma_{xz}^{(0)}|_{x=0,L} = \tilde{\sigma}_{xz}^{(0)} \text{ or } w^{(0)} \text{ is prescribed} \tag{8c}$$

where the terms $\tilde{\sigma}_{xx}^{(i)}, \tilde{\sigma}_{x\beta}^{(i)}, \tilde{\sigma}_{xz}^{(0)}; i = 0,1$ denote shell stresses on the $x = 0$ and L faces of the cylinder.

Solution

Let θ denote the wrap angle of the fibers. As illustrated in Fig. 1, θ is measured about the z direction from the parallel to the axis of rotation of the shell. When the fiber orientation is other than $\theta = n\pi/2$ $(n = 0, 1)$, the cylinder behaves as though it were fully anisotropic. For this case the classical solution using Fourier series must be modified. This is directly due to the anisotropic compliances E_{14}, E_{24}, and E_{56}§ appearing in the governing differential equations. Although it is possible to transform Eqs. (5) to one of the canonical forms, the associated change in the domain of definition distorts the bounding surfaces of the cylinder. To obtain a solution, we shall use the procedure recently discussed by Padovan[7,8] and Padovan and Lestingi.[9]

To simplify the present analysis we assume that all the surface and boundary tractions satisfy Dirichlet's conditions. Since $u^{(0)}, u^{(1)}, \ldots, w^{(0)}$ are periodic in β, they can be formally expanded in the following complex form of Fourier series

$$\zeta\,(x,\beta) = \sum_{M=-\infty}^{\infty} \zeta_M(x)e^{iM\beta} \tag{9}$$

where $i = (-1)^{1/2}$ such that

$$\zeta_M = \frac{1}{2\pi}\int_0^{2\pi} \zeta(x,\beta)e^{-iM\beta}\,d\beta \tag{10}$$

Applying Eq. (10) to Eq. (5) yields the following complex ordinary differential equation

$$B_1\zeta_{M,xx} - M^2B_2\zeta_M + iMB_3\zeta_{M,x} + B_4\zeta_{M,x} + iMB_5\zeta_M + B_6\zeta_M + \mathbf{F}_M = \mathbf{0} \tag{11}$$

where $\mathbf{F}_M$ denotes the Fourier transform of $\mathbf{F}$. The homogeneous solution of Eq. (11) may be obtained by assuming

$$\zeta_M^* \propto \chi_M \exp(\lambda_M x) \tag{12}$$

in the usual manner. Inserting Eq. (12) into Eq. (11) yields the following polynomial matrix

$$\{\lambda_M^2 B_1 + \lambda_M[B_4 + iMB_3] + B_6 - M^2B_2 + iMB_5\}\chi_M = \mathbf{0} \tag{13}$$

§ For the present paper, the material properties are obtained in the manner of Halpin and Tsai.[10]

Since B_1 is nonsingular, the pencil of Eq. (13) is regular.† In such cases, Eq. (13) implies and is implied by the partitioned matrix equation[7, 11]

$$\left[\begin{bmatrix} 0 & B_1 \\ B_1 & B_4 + iMB_3 \end{bmatrix}\lambda_M - \begin{bmatrix} B_4 + iMB_3 & 0 \\ 0 & M^2B_2 - B_6 - iMB_5 \end{bmatrix}\right]\chi_M^* = \mathbf{0} \tag{14}$$

Equation (14), which is of order ten, denotes the typically occurring linear eigenvalue problem. Since the pencil of Eq. (14) is non-Hermitian, the latent roots λ_M do not necessarily occur in conjugate pairs.

From this point the usual procedure follows. Thus the latent roots are used to construct $\zeta_m(x)$, i.e.,

$$\zeta_M(x) = \sum_{l=1}^{10} \alpha_{lM}\chi_{lM} \exp \lambda_{lM} x \tag{15}$$

where the latent vector χ_{lM} is obtained from Eq. (13) in the usual manner. The coefficients α_{lM} are obtained by substituting (15) into the transformed boundary conditions and solving the resulting complex set of linear algebraic equations. In terms of Eqs. (9) and (15), $\zeta(x,\beta)$ is thus given by

$$\zeta(x,\beta) = \sum_{M=-\infty}^{\infty}\sum_{l=1}^{10} \alpha_{lM}\chi_{lM} \exp(\lambda_{lM}x + iM\beta) \tag{16}$$

Discussion and Numerical Results

The homogeneous solution of the fully anisotropic form of Eqs. (5) and (8) has been reduced basically to a linear eigenvalue problem of a non-Hermitian pencil. The solution is "general" in the sense that arbitrary boundary conditions can be handled. For the present study, the pencil of Eq. (14) was reduced to Hessenberg form. The latent roots of the reduced matrix were subsequently obtained by the use of the numerically stable QR transformation.[12]

Since we primarily wish to illustrate the effects of anisotropy on the stress, strain and displacement fields, we have chosen a cantilevered cylindrical shell with a load on the free end of the form $\tilde{\sigma}_{xz}^{(0)} = F_M \cos 2\theta$. Figures 1 and 2 illustrate various aspects of the stress and displacement fields of the shell for various fiber orientations. For example Figs. 1 and 2 show the loci followed by the maximum values of the shell resultant $\sigma_{xz}^{(1)}$ and the radial displacement $w^{(0)}$ for the several values of θ. As expected, for the orthotropic case ($\theta = n\pi/2$), the loci occur along the lines $\beta = 0$ and π for $0 \leq x \leq L$. For the anisotropic case ($\theta \neq n\pi/2$), the loci no longer are parallel to the x axis. In fact, for $\sigma_{xz}^{(1)}$, large deviations from the orthotropic loci are noted even for small values of θ.

The contrasts between the behavior of orthotropic and anisotropic fiber reinforced single layered cylindrical shells are extremely significant as evidenced from the preceding examples. These differences have to some extent been exaggerated by the single layered nature of the shell. Obviously, the difference between the gross mechanical behavior of laminated shells with orthotropic or anisotropic lamina will be somewhat diminished.

References

[1] Gulati, S. T. and Essenburg, F., "Effects of Anisotropy in Axisymmetric Cylindrical Shells," *Journal of Applied Mechanics*, Vol. 34, Sept. 1967, pp. 659–666.

† Classical shell theory leads to an irregular pencil which is somewhat harder to handle in the computational sense.

[2] Vasilenko, A. T. "The Stress State of Antisymmetrically Loaded Shells of Revolution," *Soviet Applied Mechanics*, Engl. transl., Vol. 3, 1967, translated 1970, pp. 35–39.
[3] Whitney, J. M., "On the Use of Shell Theory for Determining Stresses in Composite Cylinders," *Journal of Composite Materials*, Vol. 5, July 1971, pp. 340–353.
[4] Bert, C. W. and Egle, D. M., "Dynamics of Composite Sandwich and Stiffened Shell-Type Structures," *Journal of Spacecraft and Rockets*, Vol. 6, No. 12, Dec. 1969, pp. 1345–1361.
[5] Flügge, W., *Stresses in Shells*, 2nd printing, Springer-Verlag Berlin, 1967.
[6] Padovan, J. and Koplik, B., "Vibrations of Closed and Open Sandwich Cylindrical Shells Using Refined Theory," *Journal of Accoustical Society of America*, Vol. 47, No. 3, Pt. 2, March 1970, pp. 862–869.
[7] Padovan, J., "Frequency and Buckling Eigenvalues of Anisotropic Cylinders Subjected to Non-uniform Lateral Prestress," *International Journal of Solids and Structures*, 1971, Vol. 7, pp. 1449–1466.
[8] Padovan, J., "Temperature Distributions in Anisotropic Shells of Revolution," *AIAA Journal*, Vol. 10, No. 1, Jan. 1972, pp. 60–64.
[9] Padovan, J. and Lestingi, J., "On the Static Solution of Monoclinic Circular Plates," *AIAA Journal*, Vol. 9, No. 12, Dec. 1971, pp. 2473–2474.
[10] Halpin, J. C. and Tsai, S. W., "Environmental Factors in Composite Materials Design," AFML TR 67-423, Air Force Materiels Lab.
[11] Lanchester, P. *Lambda-Matrices and Vibrating Systems*, Pergamon Press, New York, 1966.
[12] Francis, J. G. F., "The QR Transformation - A Unitary Analogue to the LR Transformation," *Computer Journal*, Vol. 4, pp. 265–271, 332–345.

Maximum Thrust Nozzles

WILLIAM E. CONWAY*
University of Arizona, Tucson, Ariz.
AND
AIVARS CELMIŅŠ†
U. S. Army Aberdeen Research and Development Center, Aberdeen Proving Ground, Md.

Introduction

THIS Note shows how the shape of an axisymmetrical nozzle can be found which optimizes the thrust for a given length l. We suppose the flow to take place in the meridian plane (see Fig. 1) with abscissa x and ordinate y. The method used requires an expansion curve, TB, be given as well as the input flow into the nozzle along a right going characteristic intersecting TB at C and the x axis at E. What must be found to obtain the desired shape is the flow along a left going characteristic of the nozzle flow intersecting CE at I and $x = l$ at F. This characteristic which varies along CIE on one end and along $x = l$ on the other is to afford a maximum to the thrust integral. After obtaining the flow along IF we have data along two characteristics so that a Goursat problem can be solved. Applying the total mass flow to this solution yields the nozzle shape. This work generalizes Rao's[1] one variable end point approach and contains his special solution.

Received December 13, 1971; revision received March 29, 1972. For a more complete analysis and expanded computational results, see Ballistics Research Laboratory report 1589, May 1972.
Index categories: Nozzle and Channel Flow; Optimal Structural Design.

* Professor, Department of Mathematics: work partially completed while a scientific consultant for the U. S. Army Research Office-Durham.
† Scientist, Applied Mathematics Division, Ballistics Research Laboratories.

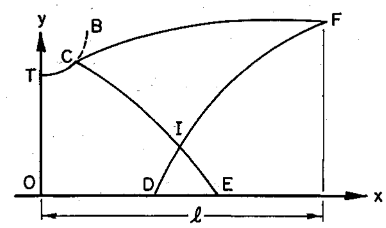

Fig. 1 Meridian plane of the nozzle.

Compressible Flow Results

Next we state results from irrotational steady supersonic flow of an ideal gas with no shock waves. The thrust, conservation of mass, nozzle length and compatibility condition are given respectively, as

$$\frac{T}{2\pi} = G(y_I) + \int_I^F y\left[p - p_0 + \frac{\rho w^2 \sin\alpha\cos\theta}{\sin(\theta+\alpha)}\right]dy \qquad (1)$$

$$m(y_F) = \beta(y_I) + \int_I^F \frac{y\rho w \sin\alpha}{\sin(\theta+\alpha)}dy = 0 \qquad (2)$$

$$l = x_c + \int_I^F \cot(\theta+\alpha)dy + L(y_I) \qquad (3)$$

$$\dot{\theta} - [(\cot\alpha)/w]\dot{w} + \sin\alpha\sin\theta/[y\sin(\theta+\alpha)] = 0 \qquad (4)$$

where $\cdot = d/dy$, w is the speed, θ is the inclination of the velocity, α is the Mach angle and p_0 is the ambient pressure. Let f_1, f_2, and f_3 be defined as the explicit integrands given in Eqs. (1), (2), and (3), respectively. Then $G(y_I)$ and $\beta(y_I)$ are integrands along EI and $L(y_I)$ is an integral along CI of f_1, f_2 and f_3, respectively, when α is replaced by $-\alpha$.

Variational Procedure

The variational method allows the use of Lagrange multipliers λ_1, λ_2, and $\lambda_4(y)$ to incorporate the constraints (2), (3) and (4). Thus we seek an extremal for the integral

$$\Phi = \int_I^F F(y,w,\dot{w},\theta,\dot{\theta},\lambda_1,\lambda_2,\lambda_4)dy + \gamma(y_I,\lambda_1,\lambda_2) \qquad (5)$$

The necessary conditions resulting from Eq. (5) are the two Euler equations for variables w and θ and the constraint (4).

At the variable end I, we suppose that y_I is free but w and θ are fixed in the sense that they must be continuous at the intersection I. This yields the transversality condition at I as

$$\frac{y_I\rho w^2 \sin 2\alpha}{\sin(\theta+\alpha)\sin(\theta-\alpha)}\left\{\frac{\sin 2\theta}{2} + \frac{\lambda_1}{w}\sin\theta - \frac{\lambda_2}{y_I\rho w^2}\right\} + \lambda_4\left\{2\dot{\Theta} - \frac{\sin^2\alpha\sin 2\theta}{y_I\sin(\theta+\alpha)\sin(\theta-\alpha)}\right\} = 0 \qquad (6)$$

where $\Theta(y)$ is the velocity inclination along CE. The condition at F is

$$t(y_F) = f + \lambda_1 f_1 + \lambda_2 f_2 = 0 \quad \text{and} \quad \lambda_4(y_F) = 0 \qquad (7)$$

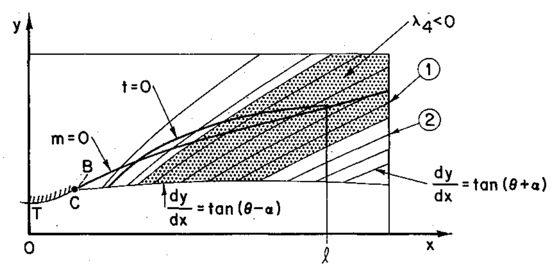

Fig. 2 Samples of characteristics with $\lambda_4 \neq 0$ which are solutions of Euler equations.